ACS APPLIED MATERIALS & INTERFACES

www.acsami.org

Research Article

Enhanced Ferromagnetism and Tunable Magnetism in Fe_3GeTe_2 Monolayer by Strain Engineering

Xiaohui Hu,* Yinghe Zhao, Xiaodong Shen, Arkady V. Krasheninnikov, Zhongfang Chen,* and Litao Sun*

Cite This: *ACS Appl. Mater. Interfaces* 2020, 12, 26367−26373

Read Online

ACCESS | Metrics & More | Article Recommendations | Supporting Information

ABSTRACT: Recent discovery of intrinsic ferromagnetism in Fe_3GeTe_2 (FGT) monolayer [Deng, Y.; et al. *Nature* 2018, *563*, 94−99; Fei, Z.; et al. *Nat. Mater.* **2018**, *17*, 778−782] not only extended the family of two-dimensional (2D) magnetic materials but also stimulated further interest in the possibility to tune their magnetic properties without changing the chemical composition or introducing defects. By means of density functional theory computations, we explore strain effects on the magnetic properties of the FGT monolayer. We demonstrate that the ferromagnetism can be largely enhanced by the tensile strain in the FGT monolayer due to the competitive effects of direct exchange and superexchange interaction. The average magnetic moments of Fe atoms increase monotonically with an increase in biaxial strain from −5 to 5% in FGT monolayer. The intriguing variation of magnetic moments with strain in the FGT monolayer is related to the charge transfer induced by the changes in the bond lengths. Given the successful fabrication of the FGT monolayer, the strain-tunable ferromagnetism in the FGT monolayer can stimulate the experimental effort in this field. This work also suggests an effective route to control the magnetic properties of the FGT monolayer. The pronounced magnetic response toward the biaxial strain can be used to design the magnetomechanical coupling spintronics devices based on FGT.

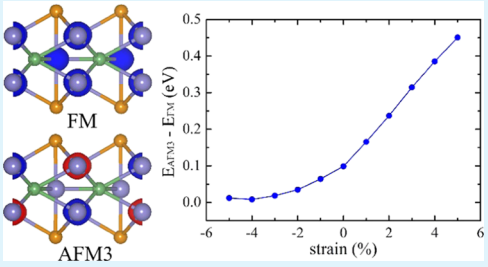

KEYWORDS: *Fe_3GeTe_2 monolayer, two-dimensional materials, ferromagnetism, magnetic properties, strain engineering*

INTRODUCTION

Two-dimensional (2D) materials, such as graphene, boron nitride, ternary boron−carbon−nitrogen systems, and transition-metal dichalcogenides, have demonstrated their great potentials in nanoelectronics due to their fascinating properties.[1−4] However, these materials are nonmagnetic, which limits their use in spintronic devices. Encouragingly, first-principles calculations indicated that magnetism can be induced in these systems by defects and/or impurities.[5−10] Thus, significant efforts have been made to introduce magnetism through defect engineering, e.g., by cutting graphene into ribbons,[11] introducing transition-metal atoms,[12,13] and creating vacancy defects[14,15] in these 2D materials. Unfortunately, although localized magnetic moments can be created using these methods, it is difficult to introduce long-range ferromagnetic ordering in these nonmagnetic 2D materials.

The very recently experimentally realized 2D materials with intrinsic ferromagnetic ordering can help overcome all these limitations, providing them with great potentials for new spintronics applications.[16−19] It has been experimentally demonstrated that monolayer CrI_3 is an Ising ferromagnet with an out-of-plane spin orientation and a Curie temperature of 45 K.[20] A recent study has shown that ferromagnetic order is present in the ultrathin layered material $Cr_2Ge_2Te_6$ at low temperatures.[21] The magnetism in bilayer CrI_3 and few-layered $Cr_2Ge_2Te_6$ can be further controlled by electric field.[22−24] In addition to CrI_3 and $Cr_2Ge_2Te_6$, other novel 2D ferromagnets have been proposed.[25−27] Among these 2D ferromagnetic materials, Fe_3GeTe_2 (FGT) is particularly promising,[28−30] as ferromagnetism persists in FGT down to the monolayer, and the Curie temperature of the FGT monolayer is 130 K, which is higher than that of other 2D ferromagnetic materials found experimentally.[28,30] Although 2D ferromagnetic order has been found experimentally in the FGT monolayer, the use of this system in actual applications requires the ability to tune its magnetic properties and enhance the stability of the ferromagnetism. Thus, achieving precise control over magnetic moments and ferromagnetic stability through external parameters is highly desirable for the practical applications of this material in spintronics.

Strain engineering, sometimes referred to as "straintronics",[31] is a promising route to modulate the electronic

Received: March 24, 2020
Accepted: May 15, 2020
Published: May 15, 2020

https://dx.doi.org/10.1021/acsami.0c05530
ACS Appl. Mater. Interfaces 2020, 12, 26367−26373

and magnetic properties of 2D materials.[32−39] It has been demonstrated that graphene can be tuned from metallic to insulating by applying strain along different crystallographic directions.[32,33] The optical band gap of MoS_2 membranes can be continuously tuned by an applied biaxial strain.[34] It was predicted that the tensile strain along the zigzag direction can greatly enhance the ferromagnetic stability of graphene with a topological line defect, while the tensile strain along the armchair direction quickly reduces magnetic moments.[36] The half-fluorinated BN and GaN layers exhibit an interesting magnetic transition from antiferromagnetism to ferromagnetism by applying strain, and a half-metallic behavior can be achieved at the 6% compression.[37] Likewise, ferromagnetism was predicted in layered NbS_2 and $NbSe_2$ under a biaxial tensile strain.[38] The induced magnetic moments can also be obviously enhanced by the tensile strain. In the VX_2 monolayers (X = S, Se), the magnetic coupling and magnetic moments were predicted to increase rapidly with increasing strain, which arises from strong ionic−covalent bonds.[39] These results strongly indicate that a systematic study of the strain effect on the magnetic behavior of the FGT monolayer is highly desirable.

In this work, by means of density functional theory (DFT) calculations, we explore the strain effect on the magnetic properties of the FGT monolayer. We show that the tensile strain can considerably enhance the ferromagnetism of the FGT monolayer. The strain-tunable ferromagnetism in the FGT monolayer predicted in our simulations can stimulate the experimental effort in this field. In addition, the average magnetic moments of Fe atoms increase monotonically with increasing strain from −5 to 5% in the FGT monolayer. The result suggests that strain engineering is an effective route to achieve large tunability of magnetic properties in the FGT monolayer.

COMPUTATIONAL METHOD

Our DFT calculations were performed using the VASP package[40,41] within the projector-augmented wave (PAW) method.[42,43] Spin-polarized local density approximation (LDA)[44] was used as the exchange-correlation functional. The previous studies[30,45] have demonstrated that LDA + U, PBE, and PBE + U functionals overestimate the magnetic moments for bulk FGT and FGT monolayer, whereas LDA can accurately describe the FGT system.[46−48] Hence, the LDA functional was chosen in our work. The energy cutoff of the plane wave basis set was 600 eV. The structures were relaxed until the energy and the force on each atom were less than 10^{-5} eV and 0.005 eV/Å, respectively. The k-point sampling of 29 × 29 × 1 was used for the unit cell of the FGT monolayer, and a 10 × 20 × 1 k-point mesh was used for the 2 × 1 × 1 supercell. A vacuum spacing of 16 Å was introduced to avoid the interlayer interactions between the periodic images of the system.

RESULTS AND DISCUSSION

The FGT monolayer has been successfully fabricated by Xu's[28] and Zhang's groups.[30] The FGT monolayer is composed of five atomic layers: the top and bottom sublayers are Te atoms, the second and fourth sublayers are Fe1 and Fe2 atoms, and the middle sublayer is made up of Fe3 and Ge atoms (Figure 1a). There are two inequivalent Fe sites in the FGT monolayer, where Fe1 and Fe2 atoms are located at the equivalent sites, while Fe3 atom has the inequivalent site. Our DFT calculation showed that the lattice parameter of the FGT monolayer is 3.91 Å, which is in a good agreement with the previous results.[30,45,49] The bond lengths and the bond angles are presented in Table S1 of the Supporting Information. Spin-density distribution in the FGT monolayer (Figure S1, Supporting Information) indicates that the magnetic moments dominantly localize on Fe atoms, and the average local magnetic moment of Fe atoms is 1.53 μ_B, which agrees with the previous studies.[30,45,49] The spin-polarized band structure of the FGT monolayer (Figure 1b) exhibits a metallic behavior for the spin-up and spin-down channels, similar to its bulk. The partial density of states (PDOS) analysis (Figure S2, Supporting Information) indicates that the Fe d orbitals mainly contribute to the metallicity.

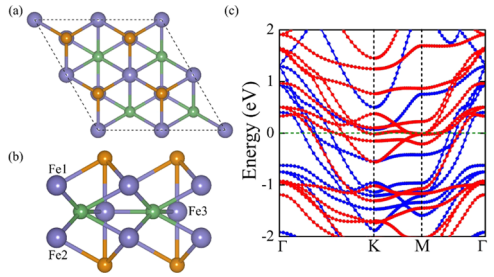

Figure 1. (a) Top and (b) side views of the structural models of the FGT monolayer. The purple, green, and yellow balls stand for Fe, Ge, and Te atoms, respectively. Fe sites are numbered by Fe1, Fe2, and Fe3, respectively, where Fe1 and Fe2 atoms are located at 2 equiv sites, while Fe3 atom has the inequivalent site. (c) Spin-polarized band structures of the FGT monolayer. The blue and red dot lines denote spin-up and spin-down channels, respectively. The Fermi level is set at zero, denoted by the olive dashed line.

The FGT monolayer is known to have a ferromagnetic (FM) coupling of magnetic moments localized on Fe atoms, and the FM-ordered spin is more desirable in practical applications in spintronic devices. However, it is not clear how the strain influences the FM spin ordering of the FGT monolayer. Therefore, we studied strain effect on the stability of ferromagnetism in the FGT monolayer. The strain effects were modeled by applying the in-plane biaxial strain along the lattice vectors. The biaxial strain is defined as $\varepsilon = \Delta c/c_0$, where c_0 and $c = c_0 \pm \Delta c$ are the unstrained and strained lattice constants of the FGT monolayer, respectively. To examine the stability of the FGT monolayer under the tensile and compressive strains, we perform the phonon spectrum calculation of the FGT monolayer at −5, −3, 0, 3, and 5% strains, respectively. It can be seen from Figure S3a−d that the FGT monolayer is dynamically stable at −3, 0, 3, and 5% strains. However, it is evident from Figure S3e that the FGT monolayer is unstable at −5% compressive strain. It can thus be concluded that the FGT monolayer is dynamically stable under the tensile strain and moderate compressive strain but unstable at large compressive strain. We note, experimentally, strain engineering of 2D materials is done by transferring the 2D material on a flexible substrate[50] making use of lattice constant or thermal-expansion mismatch. The substrate can then increase the stability of the FGT monolayer. Therefore, following the previous theoretical studies,[37,39] we explore the stability of ferromagnetism in the FGT monolayer with a strain from −5% (compressive) to 5% (tensile).

https://dx.doi.org/10.1021/acsami.0c05530
ACS Appl. Mater. Interfaces 2020, 12, 26367−26373

To investigate the magnetic couplings between the magnetic moments localized on Fe atoms, we examine the spin configurations for the FGT monolayer using a 2 × 1 × 1 supercell. According to the spin ordering of Fe atoms, four typical magnetic structures were considered, which are depicted in Figure 2a: (i) the FM state, with FM spin ordering

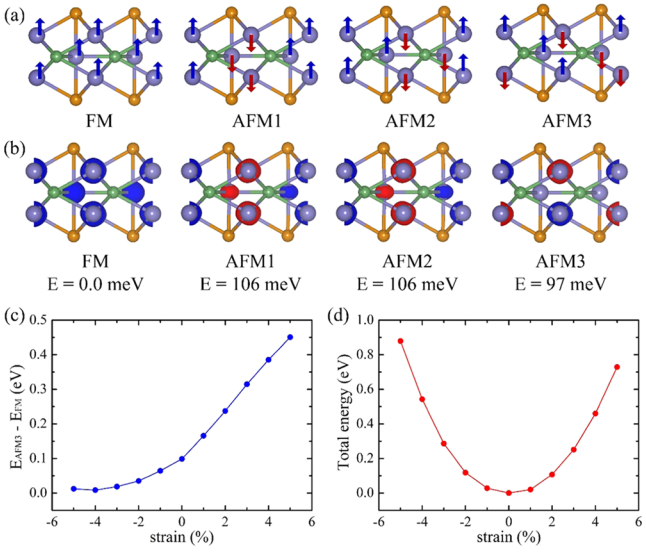

Figure 2. (a) Four different magnetic configurations and (b) spin-density distribution in the FGT monolayer, depicted as FM, AFM1, AFM2, and AFM3. (c) Energy difference between AFM3 and FM coupling and (d) the total energy as a function of the applied strain in the FGT monolayer.

at each Fe atoms, denoted by FM; (ii) the antiferromagnetic (AFM) state, with FM spin ordering at Fe1 and Fe2 atoms, the AFM spin ordering with Fe3 atom in the same cell, but with opposite ordering in the different cell, denoted by AFM1; (iii) the AFM state, with FM-ordered spins at Fe1, Fe2, and Fe3 atoms in the same cell, but with opposite ordering in the different cell, denoted by AFM2; (iv) the AFM state, with FM spin ordering at Fe1 and Fe3 atoms, AFM spin ordering with Fe2 atom in the same cell, but with opposite ordering in the different cell, denoted by AFM3. Figure 2b displays the spin density distribution of the four magnetic structures. Note that the AFM2 configuration in the FGT monolayer is not stable, and it will transfer to the AFM1 coupling after geometry optimization (see Figure 2b). The FM coupling is the lowest energy state, which is more stable than the AFM1 and AFM3 configurations by an energy difference of 106 and 97 meV, respectively. We also construct other representative AFM configurations, such as AFM4, AFM5, AFM6, and AFM7 (Figure S4, Supporting Information). It is found that these AFM configurations in the FGT monolayer are not stable.

The energy difference $\Delta E = E_{AFM3} - E_{FM}$ at various strain values is presented in Figure 2c. Here, E_{AFM3} and E_{FM} are the total energies of the AFM3 and FM configurations, respectively. It is found that the energy difference exhibits a significant increase with increasing strain from −5 to 5% for the FGT monolayer. As the tensile strain increases, the energy difference rapidly increases and reaches 451 meV at 5% strain, nearly 5 times higher than that in the unstrained FGT. At the same time, the FM stability of the FGT monolayer is remarkably enhanced, as evidenced by the increased energy difference with tensile strain. However, for the compressive strain on FGT, the energy difference decreases with higher compression, and the FM coupling is weakened. This indicates that the tensile strain can significantly enhance the FM stability of the FGT monolayer.

To understand if the FM coupling could be experimentally implemented, we considered a possible structural breakage in the considered range of strain. Figure 2d exhibits the variation of strain energy with applied strain: the strain energy is a quadratic function of strain. This indicates that the FM coupling holds in the elastic range, which has potential applications in electromechanical nanodevices.

The stability of FM coupling can be understood using the Goodenough−Kanamori−Anderson (GKA) rules.[51−53] The magnetic ground state of the FGT monolayer is governed by the direct exchange interaction and the superexchange interaction. For the direct exchange interaction, the d orbitals on the nearest-neighbor Fe atoms overlap directly, without a mediation atom. Thus, it gives rise to AFM coupling, which is governed by the distance between the neighboring Fe atoms. On the other hand, for the superexchange interaction, the d orbitals on the nearest-neighbor Fe atoms overlap with the p orbitals of Ge or Te atoms. Consequently, the superexchange mediated by Ge or Te atoms gives rise to FM coupling. The FM coupling strength is mainly sensitive to the Fe−Te (Ge)−Fe angle. If superexchange interaction is stronger than direct exchange interaction, FGT exhibits FM coupling, otherwise it shows AFM coupling.

The three different paths for superexchange interaction between the nearest-neighbor Fe atoms in the FGT monolayer are shown in Figure 3a. Figure 3b,c shows the dependence of

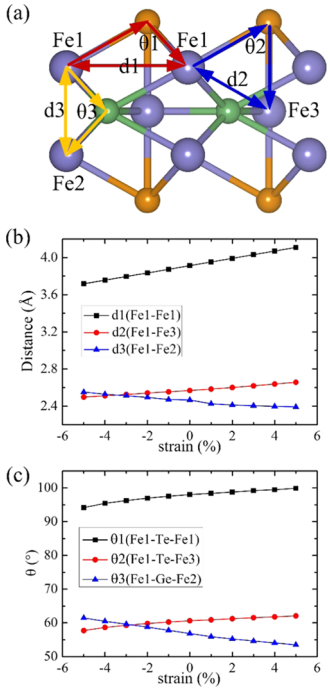

Figure 3. (a) Three different paths for superexchange interaction between the nearest-neighbor Fe atoms in the FGT monolayer. Fe1−Te−Fe1, Fe1−Te−Fe3, and Fe1−Ge−Fe2 paths are represented by red, blue, and yellow solid line triangles, respectively. Strain dependence of (b) the distance and (c) the Fe−Te (Ge)−Fe angle (Fe1−Fe1 distance, d1; Fe1−Fe3 distance, d2; Fe1−Fe2 distance, d3; Fe1−Te−Fe1 angle, θ1; Fe1−Te−Fe3 angle, θ2; Fe1−Ge−Fe2 angle, θ3).

https://dx.doi.org/10.1021/acsami.0c05530
ACS Appl. Mater. Interfaces 2020, 12, 26367−26373

the distance and the Fe−Te (Ge)−Fe angle on strain. As the strain increases, the distances of Fe1−Fe1 (d1) and Fe1−Fe3 (d2) increase, while that of Fe1−Fe2 (d3) decreases. The angles of Fe1−Te−Fe1 (θ1) and Fe1−Te−Fe3 (θ2) increase, whereas that of Fe1−Ge−Fe2 (θ3) decreases as the strain increases. The delicate balance and the competing nature of the direct exchange and superexchange interactions under the applied strain result in the stability of FM coupling. In addition, as Fe atoms have a nearly filled d-shell, there is a relatively small spatial hybridization between Fe atoms but a strong Fe−Te (Ge) covalent interaction, which leads to the direct exchange interaction being smaller than the superexchange interaction and thus a weakened AFM direct exchange, and the FM coupling becomes more stable than the AFM coupling.

To gain further insight into the magnetic properties of the FGT monolayer with applied strain, we examined the spin-density distributions (Figure 4a). Evidently, external strain has significant effect on the magnetic properties of the FGT monolayer. We further examined the strain dependence of the magnetic moments of atoms (Figure 4b,c). For simplification, the magnetic moments of Fe1 and Fe3 atoms in the FGT monolayer are named as M_{Fe1} and M_{Fe3} and that of Ge and Te atoms are named as M_{Ge} and M_{Te}, respectively. We found that M_{Fe1} increases monotonically with increase in strain from −5 to 5% in the FGT monolayer. Under tensile strain, M_{Fe1} reaches 2.26 μ_B at ε = 5%, approximately 126% increment compared to the case of undeformed FGT monolayer. For the compressive strain, M_{Fe1} decreases down to 1.46 μ_B at ε = −5%. Different from the case of M_{Fe1}, M_{Fe3} first decreases and then increases slightly with increase in strain from −5 to 5%. M_{Fe3} is calculated to be 1.33 μ_B, 1.02 μ_B, and 1.11 μ_B at ε = −5, 0, and 5%, respectively. Despite distinct changes in M_{Fe1} and M_{Fe3}, the average magnetic moment of Fe atoms increases monotonically with increasing strain from −5 to 5% in the FGT monolayer. On the other hand, M_{Ge} (M_{Te}) also increases with strain from 0.039 μ_B (0.019 μ_B) at −5% to 0.071 μ_B (0.028 μ_B) at 5%. The results suggest that Fe atoms mainly contribute spin polarizations, while Ge and Te atoms contribute little to the magnetism. The spin polarizations in the FGT monolayer are robust for a wide range of strain. As mentioned above, the structural breakage will not occur in a large elastic range. Therefore, the large elastic range will provide the possibility to modulate the spin state and the magnetic properties by applying tensile or compressive strains.

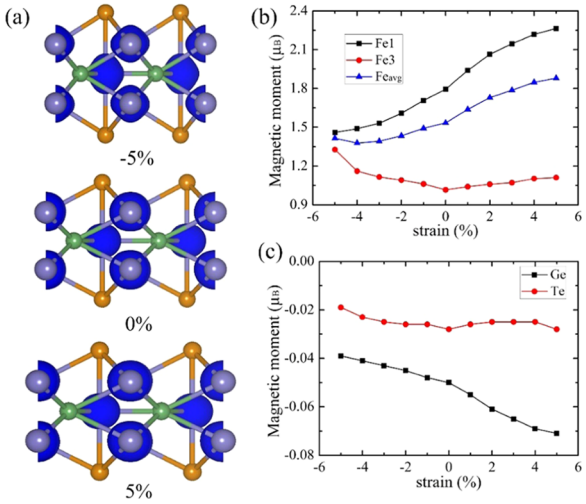

Figure 4. (a) Spin-density distribution of the FGT monolayer with −5, 0, and 5% strain. The isovalues are 0.02 e/Å^3. Strain dependence of magnetic moment (b) per Fe1 and Fe3 atoms and (c) per Ge and Te atoms in the FGT monolayer.

The interesting changes in the magnetic moments with strain can be understood by examining the bond lengths, the charge transfer, and the PDOS of the FGT monolayer under −5, 0, and 5% strain. The geometric details of the FGT monolayer under a biaxial strain are presented in Figure 5a. Due to the Poisson effect, the stretching of the in-plane biaxial direction will result in contraction in the perpendicular direction. Thus, upon applying biaxial strain on the FGT monolayer, the distance of Fe1−Fe2 and the bond length of Fe3−Te (denoted as $d_{Fe1\text{-}Fe2}$ and $d_{Fe3\text{-}Te}$) are reduced in the perpendicular direction, whereas the bond lengths of Fe1−Te and Fe3−Ge (denoted as $d_{Fe1\text{-}Te}$ and $d_{Fe3\text{-}Ge}$) increase in the plane direction. We note that the bond lengths $d_{Fe1\text{-}Te}$ and $d_{Fe3\text{-}Ge}$ increase by 5.75 and 10.53% for the FGT monolayer at a 5% tensile strain as compared to that at a −5% compressive

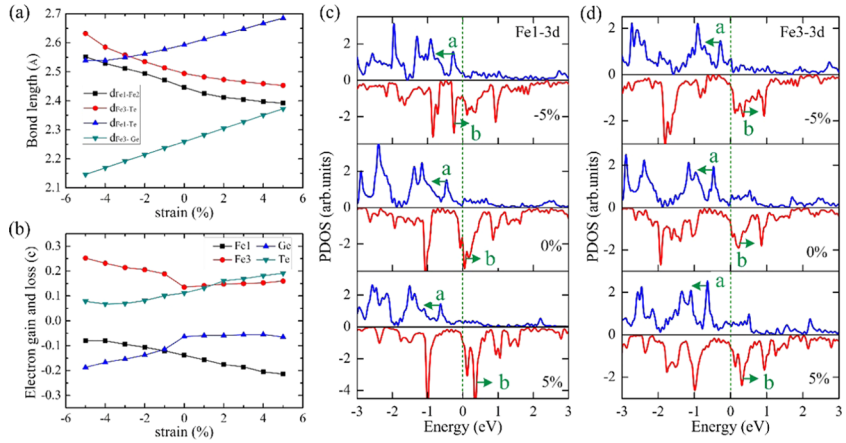

Figure 5. Strain dependence of (a) the distance and the bonding length (Fe1−Fe2 distance, $d_{Fe1\text{-}Fe2}$; Fe3−Te bond length, $d_{Fe3\text{-}Te}$; Fe1−Te bond length, $d_{Fe1\text{-}Te}$; Fe3−Ge bond length, $d_{Fe3\text{-}Ge}$). (b) Electron transfer of Fe, Ge, and Te atoms in the FGT monolayer. PDOS of (c) Fe1 atom and (d) Fe3 atom in the FGT monolayer under −5, 0, and 5% biaxial strain, respectively. The blue and red solid lines indicate spin-up and spin-down channels, respectively.

https://dx.doi.org/10.1021/acsami.0c05530
ACS Appl. Mater. Interfaces 2020, 12, 26367−26373

strain. Due to the change of the bond length, the obvious charge transfer in the FGT monolayer was observed (Figure 5b). Each Fe1 (Te) atom loses (gains) about 0.08 (0.08), 0.14 (0.11), and 0.21 (0.19) electron charge at −5, 0, and 5% strain, respectively. On the other hand, each Fe3 (Ge) atom gains (loses) about 0.25 (0.19), 0.13 (0.06), and 0.16 (0.07) electron charge at −5, 0, and 5% strain, respectively. The charge transfer between Fe1 and Te (Fe3 and Ge) atoms has a completely opposite trend, implying that the charge transfer mainly happens between Fe1 and Te (Fe3 and Ge) atoms. Furthermore, we found that the amount of charge transferred from the Fe1 atom increases monotonically, whereas that of the Fe3 atom first decreases then increases slightly with increase in strain from −5% to 5%, which has a similar trend with the change in magnetic moment of Fe1 (Fe3) atoms with strain (Figure 4b). Due to the charge transfer, it can be also seen from Figure 5c that the spin splitting of the Fe1 3d orbital near the Fermi level becomes larger with increasing strain from −5 to 5%, as is evident from the enhanced spin splitting of the a and b states in PDOS (Figure 5c), which gives rise to an increase in the magnetic moments of Fe1 atoms with strain. At the same time, for Fe3 atoms, the spin polarization is increased at −5% compressive strain and 5% tensile strain as compared to the unstrained the FGT monolayer (Figure 5d), which results in the increase in the magnetic moments of Fe3 atoms with increasing compressive and tensile strains, respectively. Therefore, the charge transfer between Fe1 and Te (Fe3 and Ge) atoms can be viewed as an important mechanism for the variation in the magnetic moment of the FGT monolayer with strain.

CONCLUSIONS

In summary, spin-polarized DFT calculations have been performed to investigate the magnetic properties of the FGT monolayer under biaxial strain. We show that the stability of ferromagnetism can be largely enhanced by the tensile strain in the FGT monolayer due to the competitive effects of direct exchange and superexchange interactions. The magnetic moments of the Fe1 atoms increase monotonically with increasing strain in the FGT monolayer, whereas the magnetic moments of the Fe3 atoms first decrease then increase slightly with change in strain from −5 to 5%. A detailed analysis revealed that the observed variation in the magnetic moment of the FGT monolayer arises from the charge transfer induced by the changes in the bond lengths under strain. Given the successful fabrication and observation of intrinsic ferromagnetism in the FGT monolayer, we strongly believe that this study will stimulate the experimental effort in this field, and strain engineering can serve as an effective way to control the magnetic properties of the FGT monolayer, which can greatly facilitate the development of spintronic devices based on 2D materials. The pronounced magnetic response toward biaxial strain in the FGT monolayer can also greatly facilitate the development of the magnetomechanical coupling spintronic devices.

ASSOCIATED CONTENT

Supporting Information

The Supporting Information is available free of charge at https://pubs.acs.org/doi/10.1021/acsami.0c05530.

Spin-density distribution, bond length, bond angle, and PDOS of the FGT monolayer; phonon spectrum of the FGT monolayer at different strains; and other representative AFM configurations (PDF)

AUTHOR INFORMATION

Corresponding Authors

Xiaohui Hu − *College of Materials Science and Engineering and Jiangsu Collaborative Innovation Center for Advanced Inorganic Function Composites, Nanjing Tech University, Nanjing 211816, China;* orcid.org/0000-0001-6346-1419; Email: xiaohui.hu@njtech.edu.cn

Zhongfang Chen − *Department of Chemistry, University of Puerto Rico, San Juan 00931, Puerto Rico;* orcid.org/0000-0002-1445-9184; Email: zhongfangchen@gmail.com

Litao Sun − *SEU-FEI Nano-Pico Center, Key Laboratory of MEMS of Ministry of Education, Collaborative Innovation Center for Micro/Nano Fabrication, Device and System, Southeast University, Nanjing 210096, China;* orcid.org/0000-0002-2750-5004; Email: slt@seu.edu.cn

Authors

Yinghe Zhao − *Department of Chemistry, University of Puerto Rico, San Juan 00931, Puerto Rico*

Xiaodong Shen − *College of Materials Science and Engineering and Jiangsu Collaborative Innovation Center for Advanced Inorganic Function Composites, Nanjing Tech University, Nanjing 211816, China*

Arkady V. Krasheninnikov − *Institute of Ion Beam Physics and Materials Research, Helmholtz-Zentrum Dresden-Rossendorf, 01314 Dresden, Germany; Department of Applied Physics, Aalto University School of Science, 00076 Aalto, Finland;* orcid.org/0000-0003-0074-7588

Complete contact information is available at: https://pubs.acs.org/10.1021/acsami.0c05530

Notes

The authors declare no competing financial interest.

ACKNOWLEDGMENTS

This work is supported in China by the National Natural Science Foundation of China (No. 11604047), the Natural Science Foundation of Jiangsu Province (No. BK20160694), the Jiangsu Planned Projects for Postdoctoral Research Funds (No. 2019K010A), the Priority Academic Program Development of Jiangsu Higher Education Institutions (PAPD), the Fundamental Research Funds for the Central Universities, and the open research fund of Key Laboratory of MEMS of Ministry of Education, Southeast University, and in USA by NSF-CREST Center for Innovation, Research and Education in Environmental Nanotechnology (CIRE2N) (Grant Number HRD-1736093). A.V.K. acknowledges funding from the German Research Foundation (DFG), project KR 48661/2. We are thankful for the computational resources from the High Performance Computing Center of Nanjing Tech University, National Supercomputer Center in Tianjin and CSC, Finland.

REFERENCES

(1) Castro Neto, A. H.; Guinea, F.; Peres, N. M. R.; Novoselov, K. S.; Geim, A. K. The Electronic Properties of Graphene. *Rev. Mod. Phys.* **2009**, *81*, 109−162.

(2) Hu, X.; Bjorkman, T.; Lipsanen, H.; Sun, L.; Krasheninnikov, A. V. Solubility of Boron, Carbon, and Nitrogen in Transition Metals: Getting Insight into Trends from First-Principles Calculations. *J. Phys. Chem. Lett.* **2015**, *6*, 3263−3268.

(3) Duan, X.; Wang, C.; Pan, A.; Yu, R.; Duan, X. Two-Dimensional Transition Metal Dichalcogenides as Atomically Thin Semiconductors: Opportunities and Challenges. *Chem. Soc. Rev.* **2015**, *44*, 8859−8876.
(4) Hu, X.; Wang, Y.; Shen, X.; Krasheninnikov, A. V.; Sun, L.; Chen, Z. 1T Phase as an Efficient Hole Injection Layer to TMDs Transistors: A Universal Approach to Achieve P-type Contacts. *2D Mater.* **2018**, *5*, No. 031012.
(5) Yazyev, O. V.; Helm, L. Defect-Induced Magnetism in Graphene. *Phys. Rev. B* **2007**, *75*, No. 125408.
(6) Santos, E. J. G.; Sánchez-Portal, D.; Ayuela, A. Magnetism of Substitutional Co Impurities in Graphene: Realization of Single π Vacancies. *Phys. Rev. B* **2010**, *81*, No. 125433.
(7) Krasheninnikov, A. V.; Lehtinen, P. O.; Foster, A. S.; Pyykko, P.; Nieminen, R. M. Embedding Transition-Metal Atoms in Graphene: Structure, Bonding, and Magnetism. *Phys. Rev. Lett.* **2009**, *102*, No. 126807.
(8) Hu, X.; Zhang, W.; Sun, L.; Krasheninnikov, A. V. Gold-Embedded Zigzag Graphene Nanoribbons as Spin Gapless Semiconductors. *Phys. Rev. B* **2012**, *86*, No. 195418.
(9) Hu, X.; Wan, N.; Sun, L.; Krasheninnikov, A. V. Semiconductor to Metal to Half-Metal Transition in Pt-Embedded Zigzag Graphene Nanoribbons. *J. Phys. Chem. C* **2014**, *118*, 16133−16139.
(10) Karthikeyan, J.; Komsa, H.; Batzill, M.; Krasheninnikov, A. V. Which Transition Metal Atoms can be Embedded into Two-Dimensional Molybdenum Dichalcogenides and Add Magnetism? *Nano Lett.* **2019**, *19*, 4581−4587.
(11) Magda, G. Z.; Jin, X.; Hagymási, I.; Vancsó, P.; Osváth, Z.; Nemes-Incze, P.; Hwang, C.; Biró, L. P.; Tapasztó, L. Room-Temperature Magnetic Order on Zigzag Edges of Narrow Graphene Nanoribbons. *Nature* **2014**, *514*, 608−611.
(12) Lin, Y.; Teng, P.; Chiu, P.; Suenaga, K. Exploring the Single Atom Spin State by Electron Spectroscopy. *Phys. Rev. Lett.* **2015**, *115*, No. 206803.
(13) Coelho, P. M.; Komsa, H. P.; Lasek, K.; Kalappattil, V.; Karthikeyan, J.; Phan, M. H.; Krasheninnikov, A. V.; Batzill, M. Room Temperature Ferromagnetism in MoTe2 by Post-Growth Incorporation of Vanadium Impurities. *Adv. Electron. Mater.* **2019**, *5*, No. 1900044.
(14) Wang, S.; Robertson, A.; Warner, J. H. Atomic Structure of Defects and Dopants in 2D Layered Transition Metal Dichalcogenides. *Chem. Soc. Rev.* **2018**, *47*, 6764−6794.
(15) Cai, L.; He, J.; Liu, Q.; Yao, T.; Chen, L.; Yan, W.; Hu, F.; Jiang, Y.; Zhao, Y.; Hu, T.; Sun, Z.; Wei, S. Vacancy-Induced Ferromagnetism of MoS2 Nanosheets. *J. Am. Chem. Soc.* **2015**, *137*, 2622−2627.
(16) Burch, K. S.; Mandrus, D.; Park, J. G. Magnetism in Two-Dimensional van der Waals Materials. *Nature* **2018**, *563*, 47.
(17) Gong, C.; Zhang, X. Two-Dimensional Magnetic Crystals and Emergent Heterostructure Devices. *Science* **2019**, *363*, No. eaav4450.
(18) Cortie, D. L.; Causer, G. L.; Rule, K. C.; Fritzsche, H.; Kreuzpaintner, W.; Klose, F. Two-Dimensional Magnets: Forgotten History and Recent Progress towards Spintronic Applications. *Adv. Funct. Mater.* **2020**, No. 1901414.
(19) Li, H.; Ruan, S.; Zeng, Y. J. Intrinsic van der Waals Magnetic Materials from Bulk to the 2D Limit: New Frontiers of Spintronics. *Adv. Mater.* **2019**, *31*, No. 1900065.
(20) Huang, B.; Clark, G.; Navarro-Moratalla, E.; Klein, D. R.; Cheng, R.; Seyler, K. L.; Zhong, D.; Schmidgall, E.; McGuire, M. A.; Cobden, D. H.; Yao, W.; Xiao, D.; Jarillo-Herrero, P.; Xu, X. Layer-Dependent Ferromagnetism in a van der Waals Crystal Down to the Monolayer Limit. *Nature* **2017**, *546*, 270−273.
(21) Gong, C.; Li, L.; Li, Z.; Ji, H.; Stern, A.; Xia, Y.; Cao, T.; Bao, W.; Wang, C.; Wang, Y.; Qiu, Z. Q.; Cava, R. J.; Louie, S. G.; Xia, J.; Zhang, X. Discovery of Intrinsic Ferromagnetism in Two-Dimensional van der Waals Crystals. *Nature* **2017**, *546*, 265−269.
(22) Jiang, S.; Li, L.; Wang, Z.; Mak, K. F.; Shan, J. Controlling Magnetism in 2D CrI3 by Electrostatic Doping. *Nat. Nanotechnol.* **2018**, *13*, 549−553.
(23) Huang, B.; Clark, G.; Klein, D. R.; MacNeill, D.; Navarro-Moratalla, E.; Seyler, K. L.; Wilson, N.; McGuire, M. A.; Cobden, D. H.; Xiao, D.; Yao, W.; Jarillo-Herrero, P.; Xu, X. Electrical Control of 2D Magnetism in Bilayer CrI3. *Nat. Nanotechnol.* **2018**, *13*, 544−548.
(24) Wang, Z.; Zhang, T.; Ding, M.; Dong, B.; Li, Y.; Chen, M.; Li, X.; Huang, J.; Wang, H.; Zhao, X.; Li, Y.; Li, D.; Jia, C.; Sun, L.; Guo, H.; Ye, Y.; Sun, D.; Chen, Y.; Yang, T.; Zhang, J.; Ono, S.; Han, Z.; Zhang, Z. Electric-Field Control of Magnetism in a Few-Layered van der Waals Ferromagnetic Semiconductor. *Nat. Nanotechnol.* **2018**, *13*, 554−559.
(25) Miao, N.; Xu, B.; Zhu, L.; Zhou, J.; Sun, Z. 2D Intrinsic Ferromagnets from van der Waals Antiferromagnets. *J. Am. Chem. Soc.* **2018**, *140*, 2417−2420.
(26) Huang, C.; Feng, J.; Wu, F.; Ahmed, D.; Huang, B.; Xiang, H.; Deng, K.; Kan, E. Toward Intrinsic Toom-Temperature Ferromagnetism in Two-Dimensional Semiconductors. *J. Am. Chem. Soc.* **2018**, *140*, 11519−11525.
(27) Li, X.; Yang, J. Realizing Two-Dimensional Magnetic Semiconductors with Enhanced Curie Temperature by Antiaromatic Ring Based Organometallic Frameworks. *J. Am. Chem. Soc.* **2019**, *141*, 109−112.
(28) Fei, Z.; Huang, B.; Malinowski, P.; Wang, W.; Song, T.; Sanchez, J.; Yao, W.; Xiao, D.; Zhu, X.; May, A. F.; Wu, W.; Cobden, D. H.; Chu, J. H.; Xu, X. Two-Dimensional Itinerant Ferromagnetism in Atomically Thin Fe3GeTe2. *Nat. Mater.* **2018**, *17*, 778−782.
(29) Li, Q.; Yang, M.; Gong, C.; Chopdekar, R. V.; N'Diaye, A. T.; Turner, J.; Chen, G.; Schol, A.; Shafer, P.; Arenholz, E.; Schmid, A. K.; Wang, S.; Liu, K.; Gao, N.; Admasu, A. S.; Cheong, S.-W.; Hwang, C.; Li, J.; Wang, F.; Zhang, X.; Qiu, Z. Patterning-Induced Ferromagnetism of Fe3GeTe2 van der Waals Materials beyond Room Temperature. *Nano Lett.* **2018**, *18*, 5974−5980.
(30) Deng, Y.; Yu, Y.; Song, Y.; Zhang, J.; Wang, N. Z.; Sun, Z.; Yi, Y.; Wu, Y. Z.; Wu, S.; Zhu, J.; Wang, J.; Chen, X. H.; Zhang, Y. Gate-Tunable Room-Temperature Ferromagnetism in Two-Dimensional Fe3GeTe2. *Nature* **2018**, *563*, 94−99.
(31) Novoselov, K. S.; Castro Neto, A. H. Two-Dimensional Crystals-Based Heterostructures: Materials with Tailored Properties. *Phys. Scr.* **2012**, *T146*, No. 014006.
(32) Guinea, F.; Katsnelson, M. I.; Geim, A. K. Energy Gaps and a Zero-Field Quantum Hall Effect in Graphene by Strain Engineering. *Nat. Phys.* **2010**, *6*, 30−33.
(33) Levy, N.; Burke, S. A.; Meaker, K. L.; Panlasigui, M.; Zettl, A.; Guinea, F.; Castro Neto, A. H.; Crommie, M. F. Strain-Induced Pseudo-Magnetic Fields Greater than 300 Tesla in Graphene Nanobubbles. *Science* **2010**, *329*, 544−547.
(34) Lloyd, D.; Liu, X.; Christopher, J. W.; Cantley, L.; Wadehra, A.; Kim, B. L.; Goldberg, B. B.; Swan, A. K.; Bunch, J. S. Band Gap Engineering with Ultralarge Biaxial Strains in Suspended Monolayer MoS2. *Nano Lett.* **2016**, *16*, 5836−5841.
(35) Molle, A.; Goldberger, J.; Houssa, M.; Xu, Y.; Zhang, S. C.; Akinwande, D. Buckled Two-Dimensional Xene Sheets. *Nat. Mater.* **2017**, *16*, 163−169.
(36) Kou, L.; Tang, C.; Guo, W.; Chen, C. Tunable Magnetism in Strained Graphene with Topological Line Defect. *ACS Nano* **2011**, *5*, 1012−1017.
(37) Ma, Y.; Dai, Y.; Guo, M.; Niu, C.; Yu, L.; Huang, B. Strain-Induced Magnetic Transitions in Half-Fluorinated Single Layers of BN, GaN and Graphene. *Nanoscale* **2011**, *3*, 2301.
(38) Zhou, Y.; Wang, Z.; Yang, P.; Zu, X.; Yang, L.; Sun, X.; Gao, F. Tensile Strain Switched Ferromagnetism in Layered NbS2 and NbSe2. *ACS Nano* **2012**, *6*, 9727−9736.
(39) Ma, Y.; Dai, Y.; Guo, M.; Niu, C.; Zhu, Y.; Huang, B. Evidence of the Existence of Magnetism in Pristine VX2 Monolayers (X = S, Se) and Their Strain-Induced Tunable Magnetic Properties. *ACS Nano* **2012**, *6*, 1695−1701.
(40) Kresse, G.; Furthmüller, J. Efficient Iterative Schemes for Ab Initio Total Energy Calculations Using a Plane-Wave Basis Set. *Phys. Rev. B* **1996**, *54*, 11169−11186.

https://dx.doi.org/10.1021/acsami.0c05530
ACS Appl. Mater. Interfaces 2020, 12, 26367−26373

(41) Kresse, G.; Furthmüller, J. Efficiency of Ab Initio Total Energy Calculations for Metals and Semiconductors Using a Plane-Wave Basis Set. *Comput. Mater. Sci.* **1996**, *6*, 15−50.
(42) Blöchl, P. E. Projector Augmented-Wave Method. *Phys. Rev. B* **1994**, *50*, 17953−17979.
(43) Kresse, G.; Joubert, D. From Ultrasoft Pseudopotentials to the Projector Augmented-Wave Method. *Phys. Rev. B* **1999**, *59*, 1758−1775.
(44) Perdew, J. P.; Zunger, A. Self-Interaction Correction to Density-Functional Approximations for Many-Electron Systems. *Phys. Rev. B* **1981**, *23*, 5048−5079.
(45) Zhuang, H. L.; Kent, P. R. C.; Hennig, R. G. Strong Anisotropy and Magnetostriction in the Two-Dimensional Stoner Ferromagnet Fe3GeTe2. *Phys. Rev. B* **2016**, *93*, No. 134407.
(46) Deiseroth, H. J.; Aleksandrov, K.; Reiner, C.; Kienle, L.; Kremer, R. K. Fe3GeTe2 and Ni3GeTe2—Two New Layered Transition-Metal Compounds: Crystal Structures, HRTEM Investigations, and Magnetic and Electrical Properties. *Eur. J. Inorg. Chem.* **2006**, 1561−1567.
(47) May, A. F.; Calder, S.; Cantoni, C.; Cao, H.; McGuire, M. A. Magnetic Structure and Phase Stability of the van der Waals Bonded Ferromagnet Fe3-xGeTe2. *Phys. Rev. B* **2016**, *93*, No. 014411.
(48) Chen, B.; Yang, J.; Wang, H.; Imai, M.; Ohta, H.; Michioka, C.; Yoshimura, K.; Fang, M. Magnetic Properties of Layered Itinerant Electron Ferromagnet Fe3GeTe2. *J. Phys. Soc. Jpn.* **2013**, *82*, No. 124711.
(49) Zhao, Y.; Gu, J.; Chen, Z. Oxygen Evolution Reaction on 2D Ferromagnetic Fe3GeTe2: Boosting the Reactivity by the Self-Reduction of Surface Hydroxyl. *Adv. Funct. Mater.* **2019**, *29*, No. 1904782.
(50) Dai, Z.; Liu, L.; Zhang, Z. Strain Engineering of 2D Materials: Issues and Opportunities at the Interface. *Adv. Mater.* **2019**, *31*, No. 1805417.
(51) Goodenough, J. B. Theory of the Role of Covalence in the Perovskite-type Manganites [La, M (II)] MoO3. *Phys. Rev.* **1955**, *100*, 564−573.
(52) Kanamori, J. Crystal Distortion in Magnetic Compounds. *J. Appl. Phys.* **1960**, *31*, S14−S23.
(53) Anderson, P. W. New Approach to the Theory of Superexchange Interactions. *Phys. Rev.* **1959**, *115*, 2−13.

https://dx.doi.org/10.1021/acsami.0c05530
ACS Appl. Mater. Interfaces 2020, 12, 26367−26373